A Prior-knowledge based Casted Shadows Prediction Model Featuring OpenStreetMap Data

M. Rogez[1,2], L. Tougne[1] and L. Robinault[1,2]
[1]*Université de Lyon, CNRS, Université Lyon 2, LIRIS, UMR5205, F-69676, Lyon, France*
[2]*Foxstream, Vaulx en Velin, France*

Keywords: Scene Modeling, Shadows Prediction, OpenStreetMap.

Abstract: We present a prior-knowledge based shadow prediction model, focused on outdoors scene, which allows to predict pixels, on the camera, which are likely to be part of shadows casted by surrounded buildings. We employ a geometrical approach which models surrounding buildings, their shadow and the camera. One innovative aspect of our method is to retrieve building datas automatically from OpenStreetMap, a community project providing free geographic data. We provide both qualitative and quantitative results in two different contexts to assess performance of our prediction model. While our method cannot achieve pixel precision easily alone, it opens opportunities for more elaborate shadow detection algorithms and occlusion-aware models.

1 INTRODUCTION

Object detection, recognition and tracking are common tasks in the video-surveillance field. Methods to achieve these tasks often rely on segmentation as a first step to extract relevant segments which can be further analyzed by computer learning methods for identification. Depending on the robustness of features chosen in the learning step, accurate segmentation might be of prime importance. Indeed under-segmentation might include pixels with very different colors which will decrease performance of colorimetric features. Furthermore, shapes features might suffer as well from over- or under-segmentation.

One of the main challenge to address to obtain accurate segmentation is shadows. Indeed, casted shadow are often undissociated from the object that cast them, especially for objects on the ground such as cars or pedestrians.

Recent shadows detection techniques have been reviewed by Sanin, Sanderson and Lovell (Sanin et al., 2012). They classify shadow detection algorithm based on the features used:

Chromaticity-based methods often use a linear color attenuation model: A shadowed pixel lowers its intensity (*ie* gets darker) without changing its chromaticity. In this context, it is often desirable to use a color space, which eases the intensity/chromaticity separation such as HSV (Cucchiara et al., 2001) or CIELAB (Lalonde et al., 2009).

Physically-based methods employ physical properties of light sources and/or physical properties of material surfaces to achieve shadow detection. Nadimi and Bhanu (Nadimi and Bhanu, 2004), for instance, model both contributions of the sun (white light) and of the sky (blue light) to build their color attenuation model. Huang and Chen (Huang and Chen, 2009) use more general illumination model called Bi Illuminant Dichromatic Reflection model to detect shadows. Finlayson, Hordley, Ku and Drew (Finlayson et al., 2002) make assumptions on the camera sensor as well to derive intrinsic image and remove shadow (Finlayson et al., 2006).

Geometric-based methods infer casted shadows from the geometric description of objects composing the current scene. These methods are often tailored for specific object shadows such as cars (Leotta and Mundy, 2006) or pedestrians. They often assume that there is only a single light source and that shadow is casted on a flat surface.

Texture-based methods assume that texture features of a given region are mostly preserved when shadowed. These methods usually work in two steps: first, they select shadow pixels candidates (a weak shadow detector is perfectly suited for this), then, correlate texture of the candidate region in the current image with the one found in the background model (Leone and Distante, 2007).

We investigate in this article another way, which explores the possibility of using contextual knowl-

602 Rogez M., Tougne L. and Robinault L..
A Prior-knowledge based Casted Shadows Prediction Model Featuring OpenStreetMap Data.
DOI: 10.5220/0004212206020607
In *Proceedings of the International Conference on Computer Vision Theory and Applications* (VISAPP-2013), pages 602-607
ISBN: 978-989-8565-47-1
Copyright © 2013 SCITEPRESS (Science and Technology Publications, Lda.)

edge easily available such as GPS coordinates of the camera and observation time to predict which pixels in the picture might be part of shadow.

We present the first step of our shadow prediction model, which estimates shadows casted by surrounding buildings. Subsequent step, would be to use such pixels predicted to be part of the shadow as a reference for shadow identification of moving objects.

One innovative aspect of our work is to include OpenStreetMap datas (OpenStreetMap contributors, 2012b) to build a geometrical scene model. Indeed other approaches, contrariwise, either build their scene model by learning it from camera observation (Jackson et al., 2004) or use premade high detailed 3d models of virtual scenes (Marin et al., 2010; Kaneva et al., 2011). More specifically, Jackson, Bodor and Papanikolopoulos (Jackson et al., 2004) unproject occlusion masks learned by cross-calibrated cameras to generate their geometric scene description; Marìn, Vazquez, Geronimo and Lopez (Marin et al., 2010) build populated virtual cities with a video game level editor and use it to train their human recognition algorithm; and Kaneva, Torralba and Freeman (Kaneva et al., 2011) use professional quality 3d virtual scene model, readily available, to assess performance of image features.

The rest of the paper is organized as follow. Section 2 presents a scene model which provides geometrical description of surrounding buildings and features OpenStreetMap data import. Section 3 describes a shadow casting algorithm and a sun position computation algorithm which produces together shadows of the above mentioned scene. Section 4 focuses on camera modeling. It describes how we produce the camera view of the scene and includes a distortion model as well. In section 5, we provide results of our shadow prediction model. We draw conclusions and share perspectives in section 6.

2 SCENE MODEL USING OPENSTREETMAP

2.1 Scene Model

The purpose of this step is to provide geometrical description of buildings surrounding the camera. We employ a deliberately simple model because it is all build from prior knowledge (*ie* data specified by the user, not from actual camera observation and learning).

First, we assume that the ground is horizontal and flat throughout the scene: there is no holes, nor terrain slope. In our formulation, the ground is defined as the plane $z = 0$.

Second, we model buildings by vertically extruded polygons. In other words, a building consists of a polygonal outline and a height (roof is flat) as shown in figure 1(a).

2.2 OpenStreetMap

While the user can define all buildings manually by specifying its outline and its height, this approach becomes tedious when more than a couple of buildings needs to be specified. That's why we investigated the possibility of using geographic data provided by the OpenStreetMap community.

Besides streets, roads or country boundaries, OpenStreetMap contains also many buildings, almost 60 millions in 2012 (OpenStreetMap contributors, 2012a), which makes it appealing for our needs.

In practice, buildings are describded by the GPS coordinates of their outline and with optionally their height. In our implementation we provide a default constant value if the buildings height is missing, but one could randomly samples the height from a Gaussian distribution to break scene uniformity.

We give in figures 1(b) and 1(c) examples of such scene model where building datas and ground map have been acquired through OpenStreetMap website.

3 SHADOW MODEL

The purpose of this model is to compute buildings cast shadows. For sake of simplicity, we consider only shadows caused by the sun and casted on the ground. Moreover, we assume that the sun behaves like a directional light. This simplification is justified because the distance between earth and sun is much bigger than typical distances involved in the scene.

With all these assumptions, plus the flat ground parametrization mentioned in the section 2.1, shadows are easily computed using parallel projection as described in (Blinn, 1988). We project building vertices on the ground plane ($z = 0$) parallely to sun direction. Such a projection can be achieved with the following matrix:

$$\begin{pmatrix} L_z & 0 & -L_x & 0 \\ 0 & L_z & -L_y & 0 \\ 0 & 0 & 0 & 0 \\ 0 & 0 & 0 & L_z \end{pmatrix} \tag{1}$$

Where $\vec{L} = (L_x, L_y, L_z)$ is the sun direction vector.

Since, we are only interested in the direction of $\vec{L}$ for shadow projection, we can impose a normalization

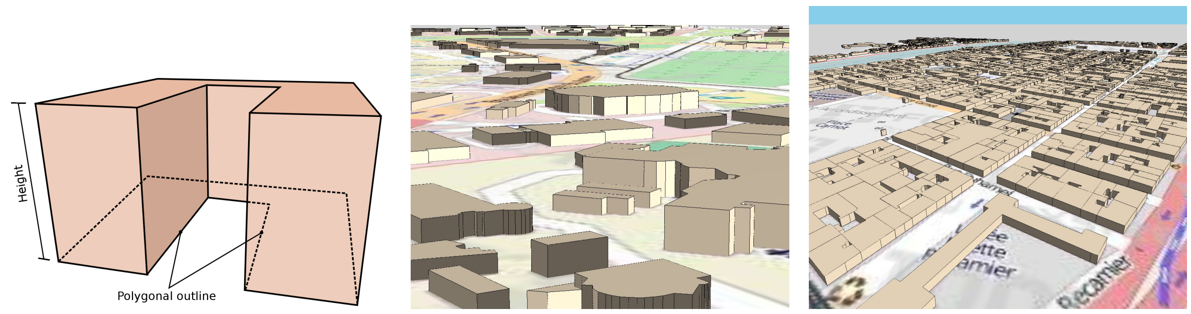

Figure 1: Figure 1(a) illustrate our building model. Figures 1(b) and 1(c) are examples of views generated by our implementation.

constraint and parametrize it with only 2 angles: azimuth and elevation which are defined relative to the north (respectively horizon) and positive toward east (respectively zenith).

3.1 Sun Position Computation Algorithm

Even if it seems easy at first glance, prediction of the sun position can be affected by many perturbations: influence of the moon causing precession and nutation, decreasing rotation speed of the earth, atmospheric refraction, *etc*. Authors have proposed various algorithms (Michalsky, 1988; Blanco-Muriel et al., 2001; Reda and Andreas, 2008; Grena, 2008) reflecting different trade-off between accuracy of prediction (within a given period of validity) and complexity of the model. Most recent work comes from (Grena, 2012) which provides five new algorithms, of various complexity, targeting the 2010-2110 period. We base our work on the third proposed algorithm because it achieves the best trade-off between accuracy (max error of 0.009°) and complexity.

Besides latitude, longitude, and time of observation (year, month, day and decimal hour), this algorithm expects temperature, pressure and $\Delta T = TT - UT$. Pressure and Temperature are used for refraction correction, whereas ΔT accounts for earth rotation irregularity. In our implementation, we have chosen, in order to reduce parameters number, to fix them to reasonable approximations: 25°C, 1 atm and 67s respectively. See `http://maia.usno.navy.mil/` for values of ΔT.

3.2 Results

In order to validate our implementation, we used datas provided by the *Institut de mécanique céleste et de calcul des éphémérides* (referred as IMCCE hereafter) as reference. However, we had to remove at-

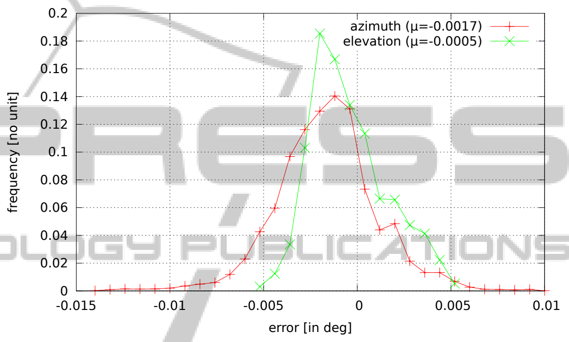

Figure 2: Error distribution of azimuth and elevation angles.

mospheric refraction correction from our implementation, for this comparison, because IMCCE dataset was built without considering such a correction.

We acquired 10000 values (1 hour spaced) of sun position during the year 2013-2014 at a specific GPS coordinate (Lyon, FRANCE) and verified that our implementation matched IMCCE dataset.

The distribution error for the year 2013 shown in figure 2 confirms the high accuracy of the algorithm: azimuth absolute error stays below 0.009°and elevation below 0.006°. However both azimuth and elevation suffer from a negative bias (-0.0017°and -0.0005°respectively). One of the possible cause of this bias is that we sample in a very narrow subdomain of algorithm parameters domain: time parameters are only taken at the very beginning of the time validity domain and localization parameters are the same for all samples.

Given the very low error on azimuth and elevation, we consider that our implementation is correct. vfill

4 CAMERA MODEL

The purpose of the camera model is to produce a synthetic view of the scene, as seen by the real camera.

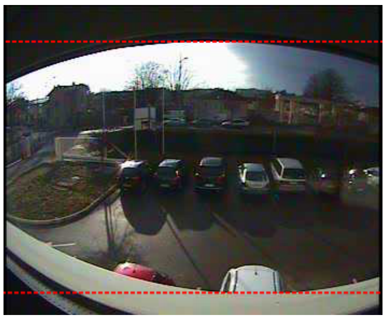
Figure 3: An example of severe lens distortion. Red dotted lines serve as a straight reference.

Because of its generality and wide use, we have chosen the Hartley-Zisserman (Hartley and Zisserman, 2003) formulation of the pinhole camera model to generate cameras views of the scene.

Furthermore, we encountered, especially in case of camera with short focals, prominent non-linear lens distortion which needed to be modelled as well, as shown in figure 3.

We employed the Brown-Conrady (Brown, 1966) distortion model which allows radial and tangential components of lens distortion to be taken into account:

$$\begin{pmatrix} x_d \\ y_d \end{pmatrix} = (1+k_1 r_u^2 + k_2 r_u^4)\begin{pmatrix} x_u \\ y_u \end{pmatrix} + \begin{pmatrix} 2p_1 x_u y_u + p_2(r_u^2 + 2x_u^2) \\ 2p_2 x_u y_u + p_1(r_u^2 + 2y_u^2) \end{pmatrix} \quad (2)$$

In equation 2, (x_u, y_u) and (x_d, y_d) denotes undistorted and distorted coordinates respectively; $r_u^2 = x_u^2 + y_u^2$ is the distance to the principal point (which is assumed to be the same as the distortion center); k_1, k_2 are the radial component parameters and p_1, p_2 are the tangential component parameters.

An illustration of the rendering with and without distortion is given in figure 4

5 RESULTS

Purpose of this section is to assess performance of our shadow prediction model. To this effect, we will compare qualitatively and quantitatively our synthetic camera view generated using OpenGL to the corresponding real camera image. We present below two examples featuring different scene contexts and time scales.

Our first example (referred as parking hereafter) shows performances of our model in an urban context where OpenStreetMap data are available. Therefore, we extracted data from OpenStreetMap and manually edited missing building heights with reasonable values (some buildings were hidden behind a wall and were therefore given a height of 0m to avoid

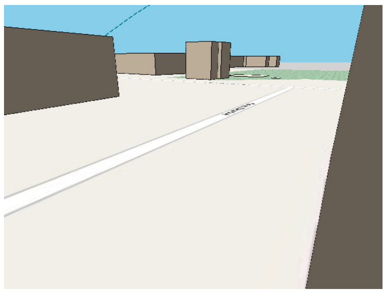
(a) Original view

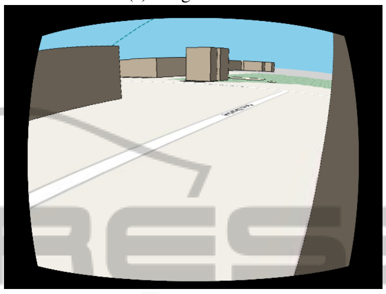
(b) Distorted view

Figure 4: Illustration of lens distortion rendering.

their effect). We set manually camera parameters to match real camera conditions. The sequence runs from 18/07/2012 14h to 19/07/2012 11h.

Our second example (referred as dam hereafter), takes place at an hydroelectric dam and shows performances on a wider time scale: we used a sequence running from 2/5/2011 to 9/27/2011. However, this time, OpenStreetMap data were not sufficient and had to be manually edited: We used a satellite view of the zone as a reference to draw the building outline. We faced furthermore a subtle problem: in our model, shadows are projected on the ground which is the plane $z = 0$. In this context it means the water is at $z = 0$. However, at the dam the water level varies (up to 3 meters according to our tests) which caused a loss of performance. To keep our model with projection plane at $z = 0$, we adapted the dam and camera height to reflect water level changes.

5.1 Qualitative Results

Visual comparison shows encouraging results for the two sequences especially when lens distortion is taken into account: shadows almost match in shape and orientation.

When lens distortion is omitted, buildings do not match the real picture and shadows are offseted. This effect is very noticeable in the first picture of first row for instance, or in upper-left corner of images from third row.

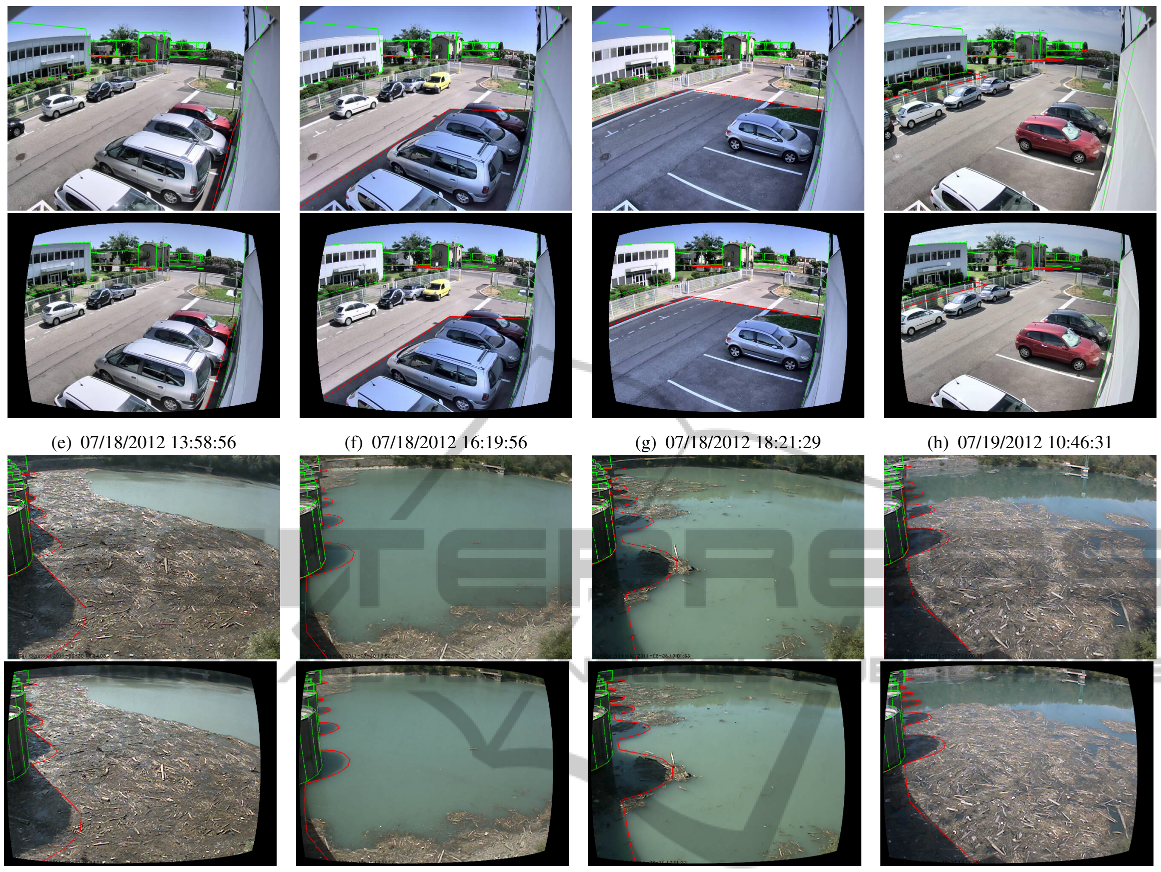

(e) 07/18/2012 13:58:56 (f) 07/18/2012 16:19:56 (g) 07/18/2012 18:21:29 (h) 07/19/2012 10:46:31

(m) 30/06/2011 18:34:08 (n) 30/07/2011 13:52:12 (o) 28/08/2011 17:01:33 (p) 27/09/2011 13:00:35

Figure 5: Visual comparison of predicted buildings (outlined in green) and corresponding shadows (outlined in red). First (resp. third) row compares prediction and real image when no distortion is applied in the parking (resp. dam) sequence. Second (resp. fourth) row compares prediction and real image when lens distortion is applied in the parking (resp. dam) sequence. (Best viewed in color).

5.2 Quantitative Results

In order to conduct our quantitative evaluation, we manually segmented building shadows casted on the ground in the camera image using the following rules:

- We discarded the black border region caused by our lens distortion implementation.
- We considered only shadows of building casted on the ground.
- When objects such as cars, fences or bushes occluded the potential ground shadow region, if there was no ambiguity, we extended known shadows boundaries, otherwise we discarded ambiguous pixels.

Then we compared our prediction and the aforementioned ground-truth on a pixel basis and derived common metrics such as Coverage Ratio (CR) (also known as Jaccard index), Precision (P), Recall (R) and F-score. We give average results for each context in table 1.

Table 1: Quantitative evaluation of performance. Row 1 and 2 (respectively 3 and 4) show results with (respectively without) lens distortion. All values are expressed in percent.

Sequence	CR	P	R	F-score
Parking	85.1	94.4	89.3	91.7
Dam	82.1	88.4	91.8	89.9
Parking	66.5	74.6	77.6	76.0
Dam	78.1	85.6	89.7	87.2

Quantitative results confirm promising results shown in the qualitative evaluation and bolster the contribution of lens distortion.

6 CONCLUSIONS

In this article we presented a prior-knowledge based building shadow prediction model which features: a scene model built with OpenStreetMap datas, a high precision shadow model and a camera model including lens distortion. We showed qualitative and quantitative results of this approach. While results are promising, pixel-precision can't be achieved easily with this sole approach, because many parameters need to be set accurately: building outlines are retrieved from OpenStreetMap which makes no guaranty of accuracy and camera calibration can be tricky especially given the high number of degree of freedom (3 for camera position, 3 for camera orientation, 5 for intrinsic parameters and 4 for lens distortion). However, we insist on the fact that this building shadow prediction model is the first step to a more general approach which will match predicted shadows to unknown moving shadows, and therefore pixel-precision results should not be required.

Furthermore, in this article we only focused on the shadow prediction part whereas much more information is available from our model. Indeed, because of the geometrical nature of our scene model, we have access to the depth map and occlusion mask quite easily. We will investigate, in future work, how can we make use of such information, especially in an object tracking context.

REFERENCES

Blanco-Muriel, M., Alarcón-Padilla, D. C., López-Moratalla, T., and Lara-Coira, M. (2001). Computing the solar vector. *Solar Energy*, 70(5):431–441.

Blinn, J. (1988). Me and my (fake) shadow. *IEEE Comput. Graph. Appl.*, 8(1):82–86.

Brown, D. C. (1966). Decentering Distortion of Lenses. *Photometric Engineering*, 32(3):444–462.

Cucchiara, R., Grana, C., Piccardi, M., Prati, A., and Sirotti, S. (2001). Improving shadow suppression in moving object detection with HSV color information. In *Intelligent Transportation Systems, 2001. Proceedings. 2001 IEEE*, pages 334–339.

Finlayson, G. D., Hordley, S. D., Lu, C., and Drew, M. S. (2002). Removing shadows from images. In *In ECCV 2002: European Conference on Computer Vision*, pages 823–836.

Finlayson, G. D., Hordley, S. D., Lu, C., and Drew, M. S. (2006). On the removal of shadows from images. *IEEE Transactions on Pattern Analysis and Machine Intelligence*, 28:59–68.

Grena, R. (2008). An algorithm for the computation of the solar position. *Solar Energy*, 82(5):462–470.

Grena, R. (2012). Five new algorithms for the computation of sun position from 2010 to 2110. *Solar Energy*, 86(5):1323–1337.

Hartley, R. and Zisserman, A. (2003). *Multiple View Geometry in Computer Vision*. Cambridge University Press, New York, NY, USA, 2 edition.

Huang, J.-B. and Chen, C.-S. (2009). Moving cast shadow detection using physics-based features. *Computer Vision and Pattern Recognition, IEEE Computer Society Conference on*, 0:2310–2317.

Jackson, B., Bodor, R., and Papanikolopoulos, N. (2004). Learning static occlusions from interactions with moving figures. In *Intelligent Robots and Systems, 2004. (IROS 2004). Proceedings. 2004 IEEE/RSJ International Conference on*, volume 1, pages 963–968 vol.1. IEEE.

Kaneva, B., Torralba, A., and Freeman, W. T. (2011). Evaluating image feaures using a photorealistic virtual world. In *IEEE International Conference on Computer Vision*.

Lalonde, J.-F., Efros, A. A., and Narasimhan, S. G. (2009). Estimating natural illumination from a single outdoor image. In *IEEE International Conference on Computer Vision*.

Leone, A. and Distante, C. (2007). Shadow detection for moving objects based on texture analysis. *Pattern Recogn.*, 40:1222–1233.

Leotta, M. J. and Mundy, J. L. (2006). Learning background and shadow appearance with 3-D vehicle models. In *Proc. British Machine Vision Conference (BMVC)*.

Marin, J., Vazquez, D., Geronimo, D., and Lopez, A. M. (2010). Learning appearance in virtual scenarios for pedestrian detection. *Computer Vision and Pattern Recognition, IEEE Computer Society Conference on*, 0:137–144.

Michalsky, J. J. (1988). The astronomical almanac's algorithm for approximate solar position (19502050). *Solar Energy*, 40(3):227–235.

Nadimi, S. and Bhanu, B. (2004). Physical models for moving shadow and object detection in video. *IEEE transactions on Pattern Analysis and Machine Intelligence (PAMI)*, 26(8).

OpenStreetMap contributors (2012a). http://taginfo.openstreetmap.org/keys/building.

OpenStreetMap contributors (2012b). http://www.openstreetmap.org.

Reda, I. and Andreas, A. (2008). Solar position algorithm for solar radiation applications.

Sanin, A., Sanderson, C., and Lovell, B. (2012). Shadow detection: A survey and comparative evaluation of recent methods. *Pattern Recognition*, 45:1684–1695.